PROBABILISTIC ANALYSIS OF EXIT GRADIENTS DUE TO STEADY SEEPAGE

By D. V. Griffiths,[1] Member, ASCE, and Gordon A. Fenton,[2] Member, ASCE

ABSTRACT: The traditional approach for estimating the exit gradient i_e downstream of water retaining structures due to steady seepage is to assume homogeneous soil properties and proceed deterministically, perhaps using flow-net techniques. Once the exit gradient is estimated, a large safety factor of at least five or six is applied. The reason for this conservative approach is twofold. First, the consequence of piping and erosion brought about by i_e approaching the critical value i_c can be very severe, leading to complete and rapid failure of civil engineering structures with little advance warning. Second, the high safety factors reflect the designer's uncertainty in local variations of soil properties at the exit points and elsewhere within the flow domain. This paper presents an alternative to the safety factor approach by expressing exit gradient predictions in the context of reliability-based design. Random field theory and finite-element techniques are combined with Monte-Carlo simulations to study the statistics of exit gradient predictions as a function of soil permeability variance and spatial correlation. Both two- and three-dimensional boundary-value problems are considered. The approach enables conclusions to be drawn about the probability of critical conditions being approached and hence failure at a given site. The reliability approach is thought to represent a more rational methodology for guiding designers in the decision-making process.

INTRODUCTION

The work presented in this paper brings together finite-element analysis and random field theory in the study of a simple boundary-value problem of steady seepage. The aim of the investigation is to observe the influence of statistically variable soil permeability on the exit gradient i_e at the downstream side of a water retaining structure in both two and three dimensions (2D and 3D). Smith and Freeze (1979, Parts 1 and 2) were among the first to study the problem of confined flow through a stochastic medium using finite differences where flow between parallel plates and beneath a single sheet pile was presented. Other workers, including the present writers [see, e.g., Griffiths and Fenton (1993, 1997)] have considered further the probabilistic seepage problem using finite-element methods for a range of boundary-value problems.

In addition to defining the soil mass as having a randomly distributed permeability k (defined here in the classical geotechnical sense as having units of length/time), the current study also includes the ability to vary the spatial correlation of the field. Spatial correlation is known to impact the results of probabilistic analyses yet rarely is taken into account in a systematic way [see, e.g., Li and Lo (1993), Mostyn and Li (1993), and White (1993)].

The use of random fields (Vanmarcke 1984; Fenton and Vanmarcke 1990) gives considerable versatility to the model in that the soil property at each location within the soil mass is itself a random variable. The random field approach therefore can appropriately take into account the positive correlation that is observed between soil properties measured at locations that are "close" together.

In previous studies of confined seepage through random soil, the seepage quantity Q has tended to be the focus of the investigations. This partly was caused by the added complexity of interpreting the first derivative of the total head (or "potential"), itself a random variable, with respect to length at the exit points. In this paper the exit gradients are studied in more detail for a range of parametric variations of the input permeability statistics. For the purposes of this initial study, a simple boundary-value problem has been considered—that of seepage beneath a single sheet pile wall penetrating to half the depth of a soil layer. Both 2D and 3D studies are presented. In 2D, it is assumed that all flow occurs in the plane of the analysis. More realistically, the 3D model has no such restriction allowing flow to occur in any direction. This particular problem has been chosen because it is well understood, and a number of theoretical solutions exist for computing flow rates and exit gradients in the deterministic (constant permeability) case [see, e.g., Harr (1962), Verruijt (1970), and Lancellotta (1993)]. Related work on hydraulic gradients within free-surface flow problems has been reported by Fenton and Griffiths (1997).

BRIEF DESCRIPTION OF FINITE-ELEMENT MODEL

In this paper a random field generator called the local average subdivision method (Fenton 1990) is combined with the finite-element method, which naturally is suited for modeling spatially varying soil properties.

The 2D finite-element mesh and dimensions are shown in Fig. 1 and the outer boundaries and dimensions of the 3D mesh are shown in Fig. 2. The 3D mesh has the same cross section in the x, y-plane as the 2D mesh (12.8 × 3.2 m) and extends by 3.2 m in the z-direction. The 2D mesh consists of square elements (0.2 × 0.2 m) and the 3D mesh consists of cubic (0.2 × 0.2 × 0.2 m) elements. The boundary conditions are such that there is a deterministic fixed total head on the upstream and downstream sides of the wall. For simplicity the head difference across the wall is set to unity. The outer boundaries of the mesh are "no-flow" boundary conditions.

In all cases, the sheet pile wall has a depth of 1.6 m, which is half the depth of the soil layer.

The finite-element program used for the solutions of Laplace's equation presented in this paper was obtained by combining Programs 5.9 and 7.0 from the modular code published in the text by Smith and Griffiths (1988). Because of the constant size elements used, an explicit form of the conductivity matrix in both 2D and 3D was employed avoiding the need for numerical integration.

Fig. 3 shows the classical smooth flow net in 2D corresponding to a constant permeability field, and Fig. 4 shows a typical case in which the permeability is distributed randomly

[1]Prof., Geomech. Res. Ctr., Colorado School of Mines, Golden, CO 80401.

[2]Assoc. Prof., Dept. of Engrg. Math., DalTech, Dalhousie, P.O. Box 1000, Halifax, Canada B3J 2X4.

Note. Discussion open until February 1, 1999. To extend the closing date one month, a written request must be filed with the ASCE Manager of Journals. The manuscript for this paper was submitted for review and possible publication on June 17, 1997. This paper is part of the ***Journal of Geotechnical and Geoenvironmental Engineering***, Vol. 124, No. 9, September, 1998. ©ASCE, ISSN 1090-0241/98/0009-0789–0797/$8.00 + $.50 per page. Paper No. 16034.

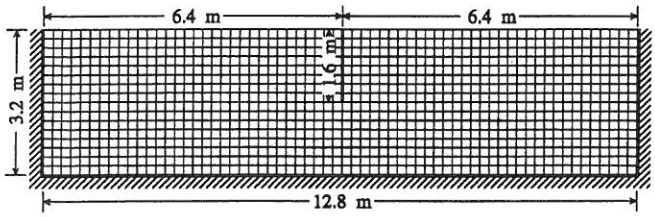

FIG. 1. Finite-Element Mesh Used for 2D Seepage Analyses

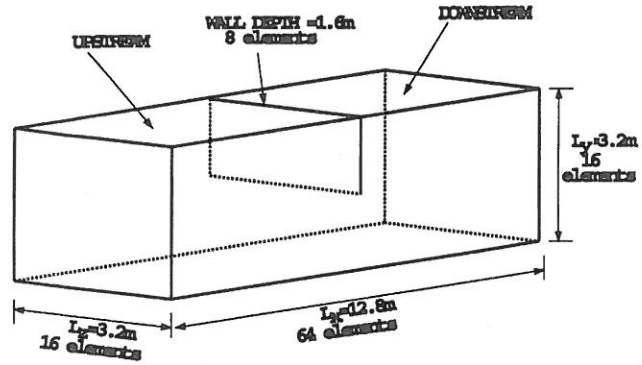

FIG. 2. Finite-Element Mesh Used for 3D Seepage Analyses (Not to Scale)

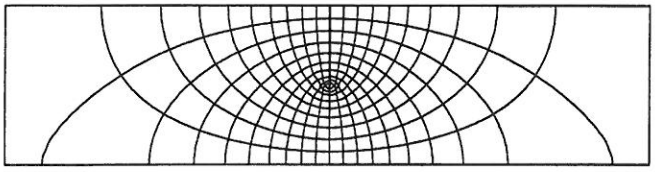

FIG. 3. Flow Net for Deterministic Analysis

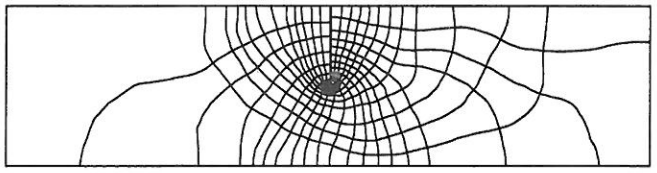

FIG. 4. Typical Flow Net with Random Permeability for Case $\theta_k = 2$ m and $COV_k = 1$

in space. In the latter case each element of the mesh has been assigned a different permeability value based on an underlying statistical distribution. Note how the flow net becomes ragged as the flow attempts to "avoid" the low permeability zones.

The exit gradient against the downstream side of the wall is computed using a two-point numerical differentiation scheme as shown in Fig. 5. The gradient is computed adjacent to the wall because this location always has the highest exit gradient in a constant permeability field and also will give the highest expected value in a random permeability field. In the 3D analyses, the exit gradient was computed at all 17 downstream locations (16 elements in the z-direction along the wall) although values computed at the center and outside edge of the wall have been the main focus of this study.

BRIEF DESCRIPTION OF THE RANDOM FIELD MODEL

Field measurements of permeability have indicated an approximately lognormal distribution [see, e.g., Hoeksema and Kitanidis (1985) and Sudicky (1986)]. The same distribution has therefore been adopted for the simulations generated in this paper.

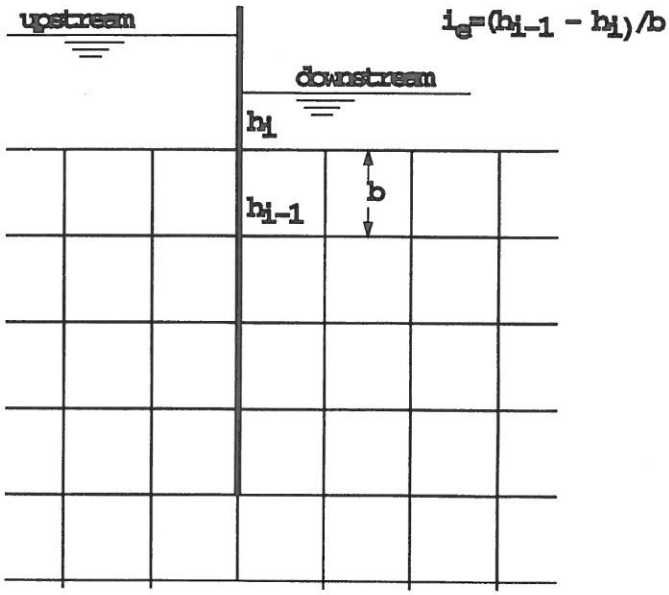

FIG. 5. Numerical Calculation of i_e

Essentially, the permeability field is obtained through the transformation

$$k_i = \exp\{\mu_{\ln k} + \sigma_{\ln k} g_i\} \quad (1)$$

where k_i = permeability assigned to the ith element; g_i = local average of a standard Gaussian random field g over the domain of the ith element; and $\mu_{\ln k}$ and $\sigma_{\ln k}$ = mean and standard deviation of the logarithm of k (obtained from the "point" mean and standard deviation μ_k and σ_k).

The local average subdivision technique (Fenton 1990; Fenton and Vanmarcke 1990) generates realizations of the local averages g_i, which are derived from the random field g having zero mean, unit variance, and a spatial correlation controlled by the scale of fluctuation θ_k. As the scale of fluctuation goes to infinity, g_i becomes equal to g_j for all elements i and j—i.e., the field of permeabilities tends to become uniform on each realization. At the other extreme, as the scale of fluctuation goes to zero, g_i and g_j become independent for all $i \neq j$—the soil permeability changes rapidly from point to point.

In the 2D and 3D analyses presented in this paper, the scales of fluctuation in the vertical, horizontal, and depth directions are taken to be equal (isotropic) for simplicity. It should be noted that for a layered soil mass the horizontal scale of fluctuation θ_h generally is larger than the vertical scale θ_v because of the natural stratification of many soil deposits. This anisotropy can be transformed to a problem with isotropic scales of fluctuation through a simple shrinking of the horizontal dimensions by the ratio of the vertical to horizontal scales of fluctuation, i.e., by scaling the horizontal coordinate by θ_v/θ_h. Such a scaling is strictly only valid for so-called ellipsoidal correlation structures, but is a reasonable approximation in any case. Thus the assumption of isotropy employed here is not a serious limitation. However, the actual spatial correlation structure of soil deposits usually is not well known, especially in the horizontal direction; hence in this paper a parametric approach has been employed to study the influence of θ_k [see, e.g., Asaoka and Grivas (1982), de Marsily (1985), and DeGroot and Baecher (1993)].

The input to the random field model therefore comprises of the three parameters (μ_k, σ_k, θ_k). Based on these underlying statistics, each of the elements (1,024 elements in the 2D case and 16,384 in the 3D case) is assigned a permeability from a realization of the permeability random field. A series of realizations is generated, each with the same underlying statistics,

but each having quite different spatial permeability patterns. The analysis of sequential realizations and the accumulation of results comprises a Monte-Carlo process. In the current study, 2,000 realizations were performed for each of the 2D cases and 1,000 in the 3D cases. The reduced number of realizations in 3D was chosen to allow a greater number of parametric studies to be performed in a reasonable time.

Following Monte-Carlo simulation of each parametric combination, 2,000 (or 1,000) values of the exit gradient i_e were obtained, which were then analyzed statistically to give the mean, standard deviation, and probability of high values occurring that might lead to piping.

The 2D model used here implies that the out-of-plane scale of fluctuation is infinite—soil properties are constant in this direction—which is equivalent to specifying that the streamlines remain in the plane of the analysis. This is clearly a deficiency; hence comparison with the 3D results will be of particular interest. An important question will be to what extent the 2D analyses represent a "reasonable" approximation.

Comparison of 2D and 3D analyses in relation to seepage quantities through spatially random soils have been reported by Griffiths and Fenton (1997).

SUMMARY OF RESULTS FROM SEEPAGE ANALYSES

The deterministic analysis of this seepage problem with a constant permeability throughout gives an exit gradient of around $i_{det} = 0.193$, which agrees closely with the analytical solution for this problem [see, e.g., Lancellotta (1993)].

Given that the critical exit gradient i_c (i.e., the value that would initiate piping) for a typical soil is approximately equal to unity, this deterministic value implies a factor of safety of around five—a conservative value not untypical of those used in design of water retaining structures [see, e.g., Harr (1962) and Holtz and Kovacs (1981)].

In all analyses the point mean permeability was fixed at $\mu_k = 1 \times 10^{-5}$ m/s whereas the point standard deviation and spatial correlation of permeability were varied in the ranges $0.03125 < \sigma_k/\mu_k < 32.0$ and $0.5 \text{ m} < \theta < 16.0$ m. For each of these parametric combinations the Monte-Carlo process led to estimated values of the mean and standard deviation of the exit gradient given by m_{i_e} and s_{i_e}, respectively. The following two sections give a summary of the results obtained in 2D and 3D, respectively.

2D

Graphs of m_{i_e} versus coefficient of variation (COV_k) and m_{i_e} versus θ_k for a range of values have been plotted in Figs. 6 and 7, respectively. Fig. 6 shows that as COV_k tends to zero, the mean exit gradient tends, as expected, to the deterministic value of 0.193. For small scales of fluctuation the mean exit gradient remains essentially constant as COV_k is increased, but for higher scales of fluctuation, the mean exit gradient tends to rise. However, the amount by which the mean exit gradient increases is dependent on θ_k and appears to reach a maximum when $\theta_k \approx 2$ m. This is shown more clearly in Fig. 7 where the same results have been plotted with θ_k along the abscissa. The maximum value of $m_{i_e} = 0.264$ recorded in this particular set of results corresponds to the case when $COV_k = 8$ and represents an increase of 37% over the deterministic value.

The return to deterministic values as θ_k increases is to be expected if one thinks of the limiting case where $\theta_k = \infty$. In this case each realization would have a constant (although different) permeability, thus the deterministic exit gradient would be obtained.

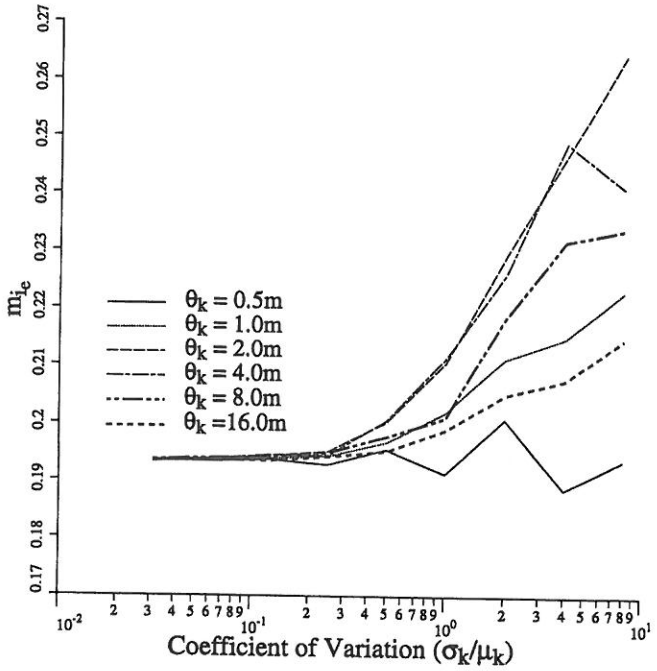

FIG. 6. Exit Gradient Mean (m_{i_e}) versus COV_k of Permeability in 2D

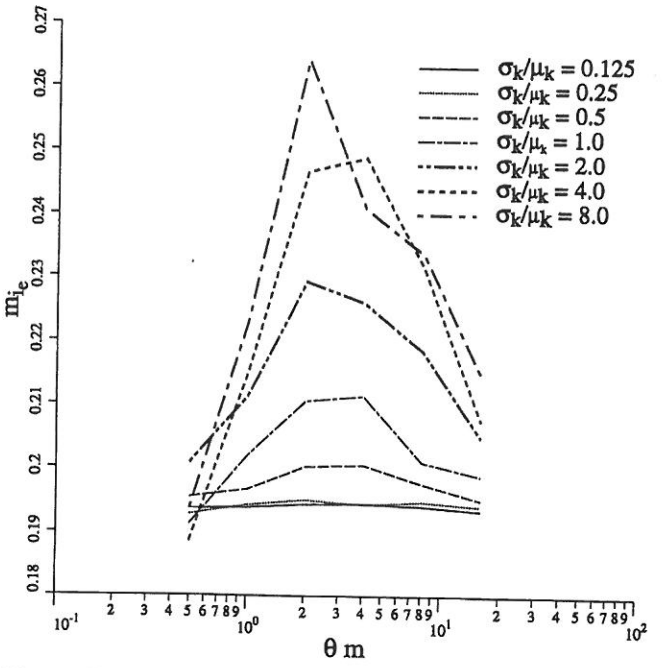

FIG. 7. Exit Gradient Mean (m_{i_e}) versus Scale of Fluctuation (θ_k) in 2D

Graphs of s_{i_e} versus COV_k and s_{i_e} versus θ_k for a same range of values have been plotted in Figs. 8 and 9, respectively. Fig. 8 shows that as COV_k increases, so the standard deviation of the exit gradient also increases. However, as was observed with the mean value of i_e, the standard deviation increases more substantially for some values of θ_k than others as shown more clearly in Fig. 9. The peak in s_{i_e} again occurs around $\theta_k \approx 2$ m.

Therefore, it would appear that there is a "worst-case" value of θ_k from a reliability-based design viewpoint in which both the mean and the standard deviation of the exit gradient reach a local maximum at the same time. At this critical value of θ_k, the higher m_{i_e} implies that on the average i_e would be closer to the critical value i_c, and to make matters worse, the higher s_{i_e} implies greater uncertainty in trying to predict i_e.

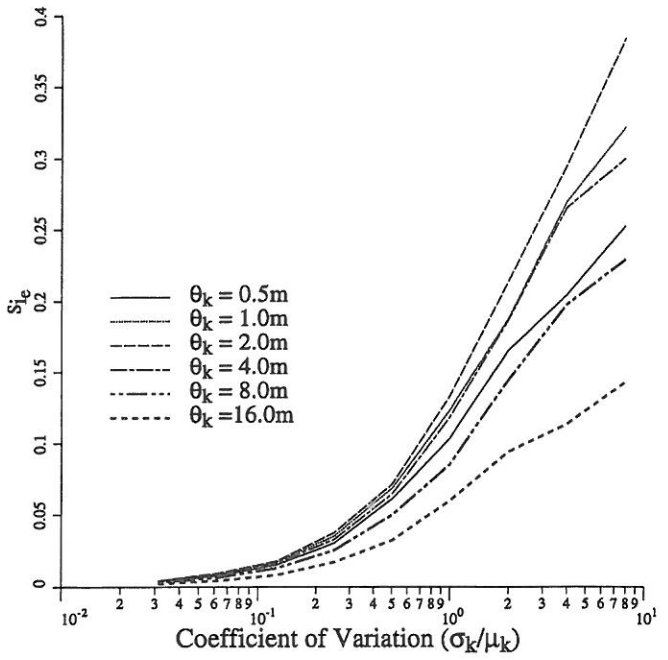

FIG. 8. Exit Gradient Standard Deviations (s_{i_e}) versus COV_k of Permeability in 2D

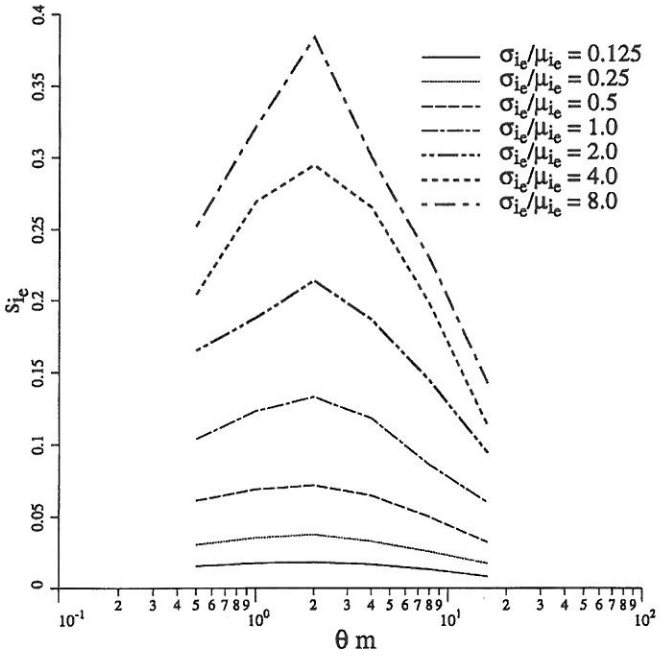

FIG. 9. Exit Gradient Standard Deviations (s_{i_e}) versus Scale of Fluctuation (θ_k) in 2D

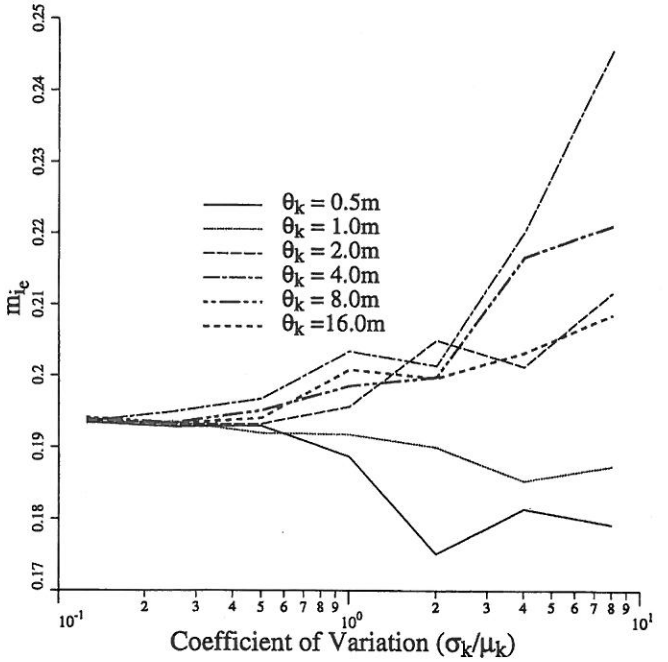

FIG. 10. Exit Gradient Mean (m_{i_e}) versus COV_k of Permeability in 3D

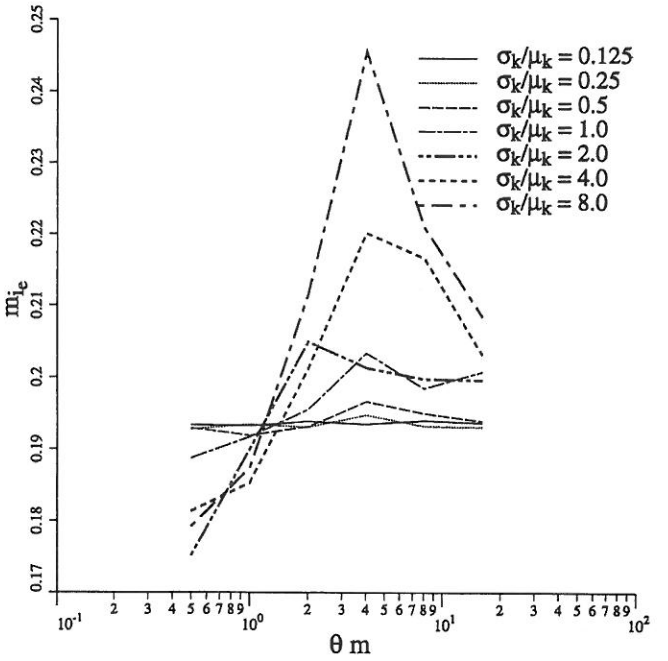

FIG. 11. Exit Gradient Mean (m_{i_e}) versus Scale of Fluctuation (θ_k) in 3D

3D

An identical set of parametric studies was performed using the 3D mesh shown in Fig. 2. The flow is now free to meander in the z-direction as it makes its primary journey beneath the wall from the upstream to the downstream side. Although the exit gradient is computed at 17 locations adjacent to the downstream side of the wall (16 elements) initial results are presented for the central location because this is considered to be the point where the effects of 3D will be greatest. Figs. 10–13 are the 3D counterparts of Figs. 6–9 in 2D.

Fig. 10 shows the variation in m_{i_e} as a function of COV_k for different θ_k values. For low values of θ_k, the mean remains constant and even starts to fall as COV_k is increased. For higher θ_k values, the mean exit gradient starts to climb, and, as was observed in 2D (Fig. 6), there is a critical value of θ_k for which the greatest values of m_{i_e} are observed. This is seen more clearly in Fig. 11 in which m_{i_e} is plotted as a function of θ_k. The maxima in m_{i_e} are seen clearly and occur at higher values of $\theta_k \approx 4$ m than in 2D (Fig. 7), which gave maxima closer to $\theta_k \approx 2$ m. The maximum value of $m_{i_e} = 0.246$ recorded in this particular set of results corresponds to the case ($COV_k = 8$, $\theta_k = 4$ m) and represents an increase of 27% over the deterministic value. This should be compared with the 37% increase observed for the same case in 2D.

Figs. 12 and 13 show the behavior of s_{i_e} as a function of COV_k and θ_k. Fig. 12 indicates that the standard deviation of the exit gradient increases with COV_k for all values of θ_k, but the extent of the increase is again dependent on the scale of

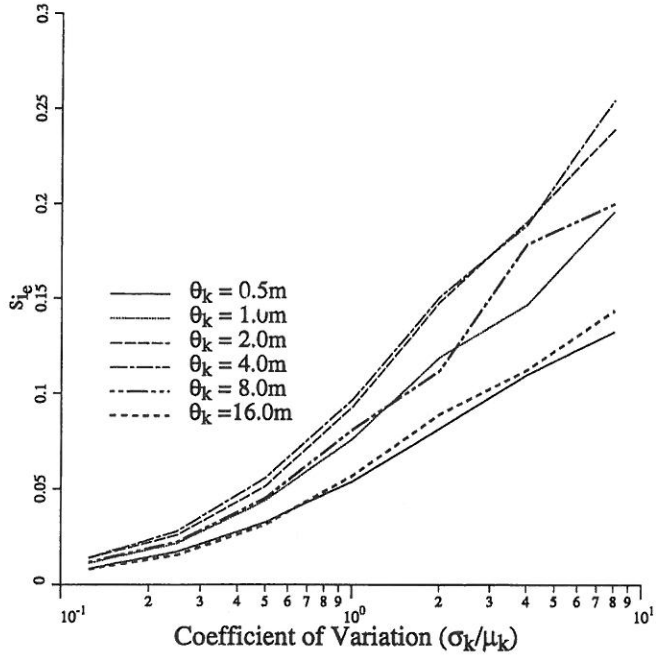

FIG. 12. Exit Gradient Standard Deviations (s_{i_e}) versus COV_k in 3D

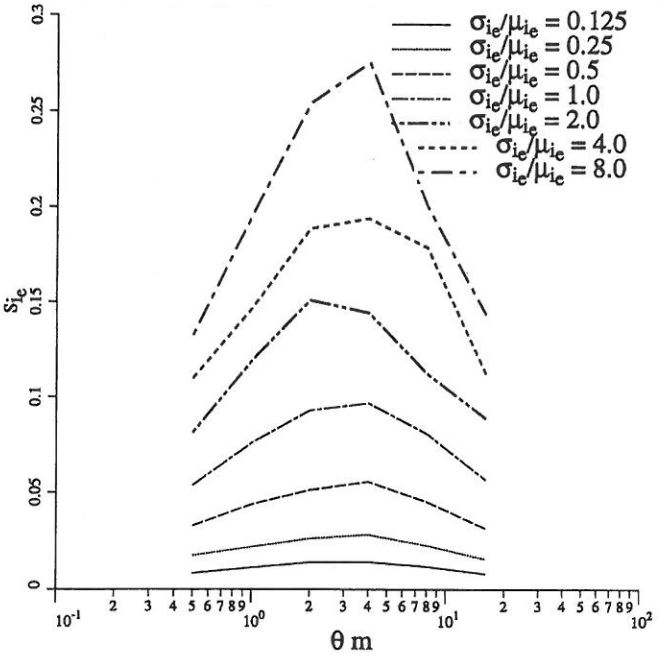

FIG. 13. Exit Gradient Standard Deviations (s_{i_e}) versus Scale of Fluctuation (θ_k) in 3D

fluctuation as shown in Fig. 13, with the maxima occurring in the range θ_k = 2–4 m.

REPRODUCIBILITY

Before proceeding it is appropriate to show evidence of the reproducibility of the results. This seems particularly important when results are presented in statistical form. In this context, the question of reproducibility is aimed at two main areas.

1. If an analysis involving a particular parametric combination and a particular number of realizations is repeated, are similar results obtained?
2. Are 1,000 realizations sufficient for statistically stable results in 3D?

In Figs. 14(a and b), two completely independent sets of

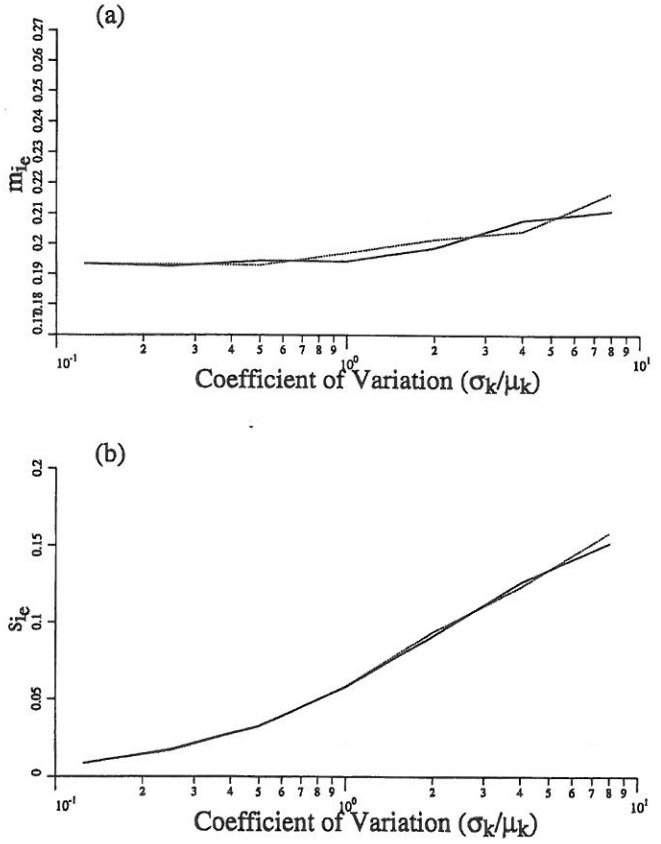

FIG. 14. For Case θ_k = 16 m in 3D (1,000 Realizations) Reproducibility of: (a) m_{i_e}; (b) s_{i_e}

results for a range of COV_k values, all obtained using 1,000 realizations, are presented for the case when θ_k = 16 m (the highest value used in the present study). This particular value of θ_k was chosen because larger values of θ_k generally require more realizations for stability. The close reproducibility of both the mean and the standard deviation of the exit gradient is indicated. Reproducibility studies of a wide range of geotechnical applications with Monte-Carlo simulations have been reported by Paice (1997).

COMPARISON OF 2D AND 3D

Compared with 2D analysis, 3D allows the flow greater freedom to avoid the low permeability zones. The influence of 3D is therefore to reduce the overall "randomness" of the results observed from one realization to the next. This implies that the sensitivity of the output quantities to COV_k will be reduced in 3D as compared with 2D. In a study of seepage quantities (Griffiths and Fenton 1997) the expected flow rate was reduced as COV_k was increased; however, this reduction was more pronounced in 2D than in 3D. Similarly, in this study of exit gradients, the change in m_{i_e} over its deterministic value with increasing COV_k is less than it was in 2D.

For the case of θ_k = 2 m, Fig. 15 presents results for m_{i_e} in both 2D and 3D. An additional 3D result corresponding to the mean exit gradient at the edge of the wall also is included. A consistent pattern is observed in which the 3D (center) result shows the smallest increase in m_{i_e} and the 2D result shows the greatest increase. An intermediate result is obtained at the edge of the wall where the flow is restrained in one direction. The boundary conditions on this plane will ensure that the edge result lies between the 2D and the 3D (center) results.

Fig. 16 presents results for s_{i_e} for the same three cases. These results are much closer together although the 3D (center) standard deviations record the lowest values.

In summary, the effect of allowing flow in 3D is to increase

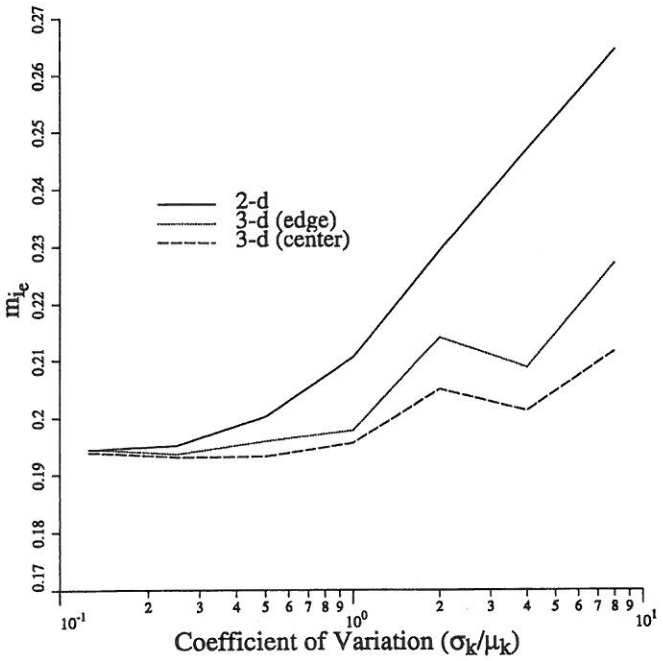

FIG. 15. Comparison of m_{i_e} in 2D and 3D ($\theta_k = 2$ m)

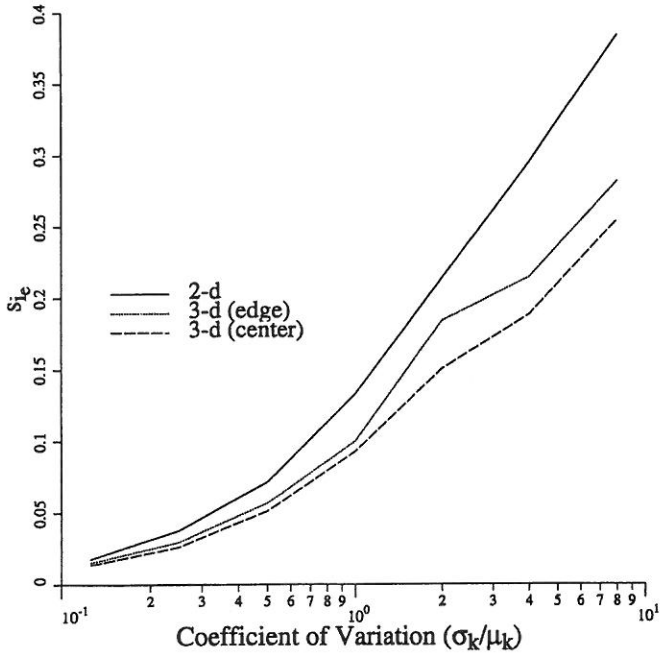

FIG. 16. Comparison of s_{i_e} in 2D and 3D ($\theta_k = 2$ m)

the averaging effect discussed earlier within each realization. However, the difference between the 2D and 3D results is not that great and it could be argued that a 2D analysis is a reasonable first approximation to the "true" behavior. In relation to the prediction of exit gradients, it also appears that 2D is conservative, in that the increase in m_{i_e} with COV_k observed for intermediate values of θ_k is greater in 2D than in 3D.

RELIABILITY-BASED DESIGN INTERPRETATION

A factor of safety applied to a deterministic prediction is intended to eliminate any serious possibility of failure but without any objective attempt to quantify the risk. Reliability-based design attempts to quantify risk by seeking answers to the following questions:

1. What is the probability that the actual exit gradient will exceed the deterministic prediction (based on constant properties throughout)?
2. What is the probability that the actual exit gradient will exceed the critical value, resulting in failure?

The Monte-Carlo scheme described in this paper enables probabilistic statements to be made. For example, if out of 1,000 realizations, 50 gave an exit gradient $i_e \geq 1$, it could be concluded that the probability of piping or erosion was of the order of 50/1,000, or 5%. In general though, a histogram can be plotted and the probabilities computed via standard tables of the area beneath a normal curve.

2D

A typical histogram of exit gradient values corresponding to $\theta_k = 2$ m and $COV_k = 1$ for a 2D analysis is shown in Fig. 17. The ragged line comes from the frequency count obtained over the realizations and the smooth dotted line is based on a lognormal fit to that data. The lognormal fit has been scaled such that the area beneath it equals unity. The good agreement suggests that the actual distribution of exit gradients is indeed lognormal. The mean and standard deviation of the underlying normal distribution of ln i_e also is printed on the figure. It should be noted that the relationships between the statistics of ln i_e and i_e are given by

$$\mu_{i_e} = \exp\left\{\mu_{\ln i_e} + \frac{1}{2}\sigma^2_{\ln i_e}\right\} \tag{2}$$

$$\sigma^2_{i_e} = \mu^2_{i_e}\{\exp(\sigma^2_{\ln i_e}) - 1\} \tag{3}$$

Because Fig. 17 shows a fitted lognormal probability density function, probabilities can be deduced directly. For example, in the particular case shown, the probability that the actual exit gradient will exceed the deterministic value of i_{det} = 0.193 is approximated by

$$P[i_e > 0.193] = 1 - \Phi\left(\frac{\ln 0.193 + 1.7508}{0.6404}\right) \tag{4}$$

where $\phi(\cdot)$ = cumulative normal distribution function. In this case $\Phi(0.17) = 0.57$, thus

$$P[i_e > 0.193] = 0.43 \tag{5}$$

and there is a 43% probability that the deterministic prediction of $i_{det} = 0.193$ is unconservative.

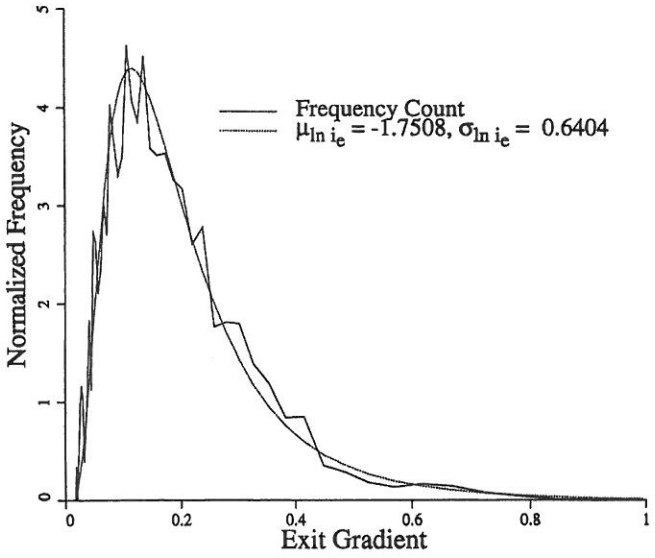

FIG. 17. Histogram of Exit Gradients in 2D for Case $\theta_k = 2$ m and $COV_k = 1$

A similar calculation has been performed for all the parametric variations considered in this study. In each case the following probability was calculated:

$$P[i_e > \alpha i_{det}] \quad (6)$$

where α = a simple scaling factor on the deterministic exit gradient. When $\alpha = 1$ [as in (5)], the result is just the probability that the actual exit gradient will exceed the deterministic value. Larger values of α are interesting for design purposes where a prediction of the probability of failure is required. In the current example, the deterministic exit gradient is approximately equal to 0.2, so it would be of interest to know the probability of the actual exit gradient exceeding the critical hydraulic gradient $i_c \approx 1$. For this comparison therefore α would be set equal to 5.

A full range of probability values in 2D has been computed in this study and some selected results will now be described. A set of probabilities corresponding to $\theta_k = 2$ m is presented in Fig. 18. The mean and standard deviation of the exit gradients reached a local maximum at this value (Figs. 7 and 9).

It should be noted that irrespective of the θ_k or COV_k, $P[i_e > i_{det}]$ is always less than 50%. This is a reassuring result from a design standpoint. The probabilities that approach 50% correspond to a very low COV_k and are somewhat misleading in that the computed exit gradients have a very low variance and are approaching the deterministic value. The 50% merely refers to an equal likelihood of the actual exit gradient lying on either side of an essentially normal distribution with a small variance and a mean of i_{det}. For small COV_k, this is shown clearly by the sudden reduction to zero of the probability that i_e exceeds i_{det} scaled up by a small factor (say 10% as indicated by $\alpha = 1.1$).

As α is increased further, the probability consistently falls, although each curve exhibits a maximum probability corresponding to a different value of COV_k. This interesting observation implies that there is a worst-case combination of θ_k and COV_k that gives the greatest likelihood of i_e exceeding i_{det}.

In consideration of failure conditions, the value of $P[i_e \geq 1]$, as indicated by the curve corresponding to $\alpha = 5$, is small but not insignificant, with probabilities approaching 10% for the highest COV_k cases considered. In view of this result, it is not surprising that for highly variable soils a factor of safety against piping of up to 10 has been suggested by some commentators [see, e.g., Harr (1987)].

3D

An examination of the central exit gradients predicted by the 3D analyses indicates that they are broadly similar to those obtained in 2D.

Fig. 19 shows a typical histogram of the central exit gradient value corresponding to $\theta_k = 2$ m and $COV_k = 1$ for a 3D analysis. This is the same parametric combination given in Fig. 17 for 2D. The fitted curve again indicates that the actual distribution of exit gradients is lognormal. The mean and standard deviation of the underlying normal distribution of ln i_e also is printed on the figure. In the case illustrated by Fig. 19, the probability that the actual exit gradient will exceed the deterministic value of $i_{det} = 0.193$ is equal to 42% and is virtually the same as the 43% given in 2D.

The probability of an unconservative design based on 3D studies of a full range of COV_k values with $\theta_k = 2$ m is shown in Fig. 20 together with the corresponding results in 2D ($\alpha = 1$). Although there are some fluctuations in the 3D results, the

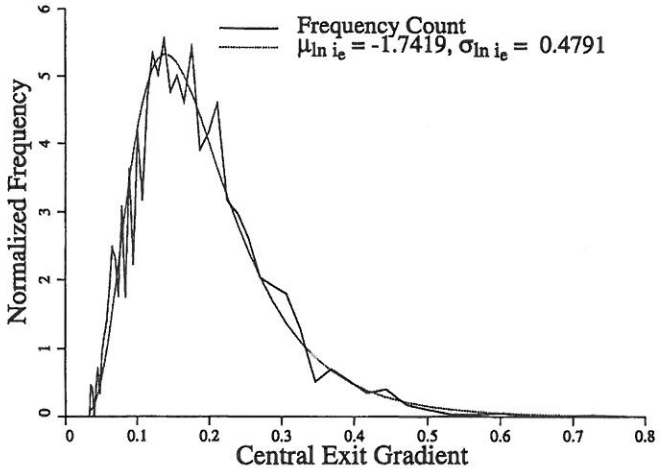

FIG. 19. Histogram of Central Exit Gradients in 3D for Case θ_k = 2 m and COV_k = 1

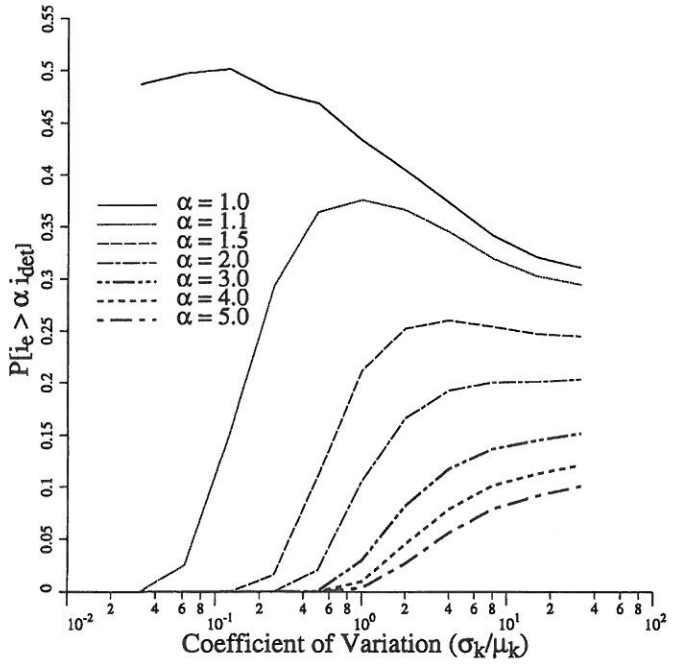

FIG. 18. Probability that i_e Exceeds αi_{det} versus COV_k for Case θ_k = 2 m in 2D

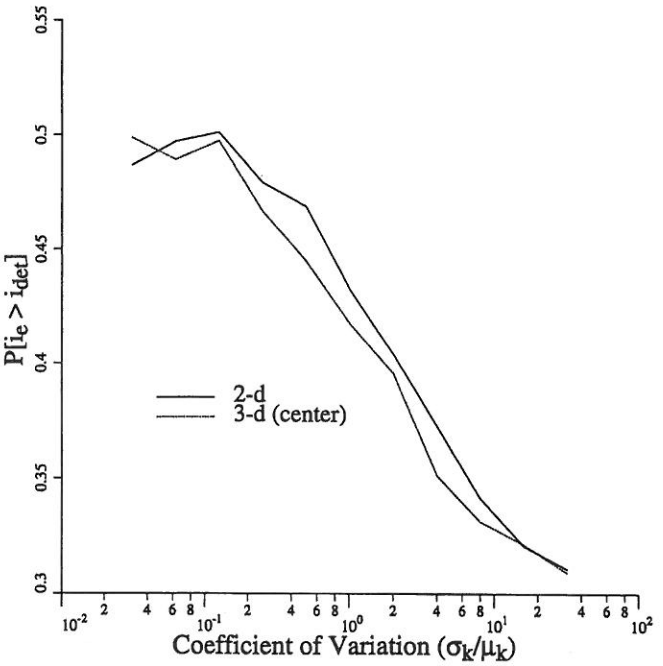

FIG. 20. Probability that i_e Exceeds i_{det} versus COV_k for Case θ_k = 2 m in 2D and 3D

overall trend indicates a slight reduction in probability values as compared with 2D. It appears that simpler and computationally less intensive 2D analysis of exit gradients will generally give sufficiently accurate and conservative reliability estimates of exit gradients.

CONCLUDING REMARKS

In this paper, random field methodology has been combined with the finite-element method to study the exit gradient caused by steady seepage beneath a single sheet pile wall embedded in a layer of random soil. The influence of spatial correlation of soil properties has been incorporated fully through a scale of fluctuation parameter θ_k. Both 2D and 3D conditions have been considered.

The spatial correlation and the COV_k of the input permeability were varied over a wide range of values. For each parametric combination, a Monte-Carlo process led to values of exit gradients on the downstream side of the wall, which were then processed statistically in the context of reliability-based design.

Generally speaking the computed variance of the exit gradient was considerably higher than other quantities of interest in the flow problem such as the flow rate. This is hardly surprising when one considers that the exit gradient is a derivative quantity, which is dependent on the total head value computed at a very specific location within the mesh at the downstream exit point.

An interesting result was that the computed exit gradient was found to reach a maximum for a particular value of the scale of fluctuation, which lay in the range θ_k = 2–4 m. The higher end of this range was observed in the 3D studies and the lower end in 2D.

When the results were interpreted in the context of reliability-based design, conclusions could be reached about the probability of exit gradient values exceeding the deterministic value or even reaching levels at which stability and piping could occur. In 2D and for the particular case of $\theta_k = 2$ m, the probability of the actual exit gradient exceeding the deterministic value could be as high as 50%, but generally lay in the 40% range for moderate values of COV_k. The probability of an unconservative deterministic prediction generally was found to exhibit a maximum point corresponding to a particular combination of θ_k and COV_k. From a design point of view this could be considered a worst-case scenario leading to maximum uncertainty in the prediction of exit gradients.

With regard to the possibility of piping, erosion, and eventual failure of the system, a relationship was established between the traditional factor of safety and the "probability of failure." For the particular case mentioned earlier and assuming that the critical exit gradient is of the order of $i_c \approx 1$, a factor of safety of five could still imply a probability of failure as high as 10% if COV_k also is high. This result suggests that factors of safety as high as 10 may not be unreasonable for critical structures founded in highly variable soil.

The 3D studies were considerably more intensive computationally than their 2D counterparts but had the modeling advantage of removing the requirement of planar flow. In 3D, the flow has greater freedom to avoid the low permeability zones; thus there is less randomness associated with each realization. This was manifested in a reduced mean and standard deviation of the exit gradient as compared with 2D. However, the differences were not that great and indicated that 2D exit gradients studies in random soils will lead to conservative results while giving sufficient accuracy.

ACKNOWLEDGMENTS

The writers acknowledge the support of National Science Foundation Grant Nos. 95-12434 and 97-13442, and National Sciences and Engineering Research Council of Canada Grant No. OPG0105445.

APPENDIX I. REFERENCES

Asaoka, A., and Grivas, D. A. (1982). "Spatial variability of the undrained strength of clays." *J. Geotech. Engrg.*, ASCE, 108(5), 743–756.

DeGroot, D. J., and Baecher, G. B. (1993). "Estimating autocovariance of in-situ soil properties." *J. Geotech. Engrg.*, ASCE, 119(1), 47–166.

de Marsily, G. (1985). "Spatial variability of properties in porous media: A stochastic approach." *Advances in transport phenomena in porous media*, J. Bear and M. Y. Corapcioglu, eds., North Atlantic Treaty Organization Advanced Study Institute on Fundamentals of Transport Phenomena in Porous Media, Dordrecht, Boston, Mass., 716–769.

Fenton, G. A. (1990). "Simulation and analysis of random fields," PhD thesis, Department of Civil Engineering and Operations Research, Princeton University, Princeton, N.J.

Fenton, G. A., and Griffiths, D. V. (1997). "Extreme hydraulic gradient statistics in a stochastic earth dam." *J. Geotech. Geoenvir. Engrg.*, ASCE, 123(11), 995–1000.

Fenton, G. A., and Vanmarcke, E. H. (1990). "Simulation of random fields via local average subdivision." *J. Engrg. Mech.*, ASCE, 116(8), 1733–1749.

Griffiths, D. V., and Fenton, G. A. (1993). "Seepage beneath water retaining structures founded on spatially random soil." *Géotechnique*, London, U.K., 43(4), 577–587.

Griffiths, D. V., and Fenton, G. A. (1997). "Three-dimensional seepage through a spatially random soil." *J. Geotech. Engrg.*, ASCE, 123(2), 153–160.

Harr, M. E. (1962). *Groundwater and seepage.* McGraw-Hill, Inc., London, New York, N.Y.

Harr, M. E. (1987). *Reliability based design in civil engineering.* McGraw-Hill, Inc., London, New York, N.Y.

Hoeksema, R. J., and Kitanidis, P. K. (1985). "Analysis of the spatial structure of properties of selected aquifers." *Water Resour. Res.*, 21(4), 563–572.

Holtz, R. D., and Kovacs, W. D. (1981). *An introduction to geotechnical engineering.* Prentice-Hall, Englewood Cliffs, N.J.

Lancellotta, R. (1993). *Geotechnical engineering.* A. A. Balkema, Rotterdam, The Netherlands.

Li, K. S., and Lo, S.-C. R., eds. (1993). *Probabilistic methods in geotechnical engineering.* A. A. Balkema, Rotterdam, The Netherlands.

Mostyn, G. R., and Li, K. S. (1993). "Probabilistic slope stability—state of play." *Proc., Conf. Probabilistic Meths. Geotech. Engrg.*, K. S. Li and S.-C. R. Lo, eds., A. A. Balkema, Rotterdam, The Netherlands, 89–110.

Paice, G. M. (1997). "Finite element analysis of stochastic soils," PhD thesis, University of Manchester, Manchester, U.K.

Smith, L., and Freeze, R. A. (1979). "Stochastic analysis of steady state groundwater flow in a bounded domain, 1. One-dimensional simulations." *Water Resour. Res.*, 15(3), 521–528.

Smith, I. M., and Griffiths, D. V. (1988). *Programming the finite element method*, 2nd ed., John Wiley & Sons, New York, N.Y.

Sudicky, E. A. (1986). "A natural gradient experiment on solute transport in a sand aquifer: Spatial variability of hydraulic conductivity and its role in the dispersion process." *Water Resour. Res.*, 22(13), 2069–2083.

Vanmarcke, E. H. (1984). *Random fields: Analysis and synthesis.* MIT Press, Cambridge, Mass.

Verruijt, A. (1970). *Theory of groundwater flow.* Macmillan and Co., Ltd, London, U.K.

White, W. (1993). "Soil variability: Characterization and modelling." *Proc., Conf. Probabilistic Meths. Geotech. Engrg.*, K. S. Li and S.-C. R. Lo, eds., A. A. Balkema, Rotterdam, The Netherlands, 111–120.

APPENDIX II. NOTATION

The following symbols are used in this paper:

b = finite-element side length;
COV_k = coefficient of variation (σ_k/μ_k);
g, g_i = local average over ith element of standard Gaussian field;
h_i, h_{i-1} = total head values at exit point;
i_c = critical exit gradient;
i_{det} = deterministic exit gradient;

i_e = exit gradient;
k_i = permeability of kth element;
L_x, L_y, L_z = mesh dimensions;
m_{i_e}, s_{i_e} = estimated mean and standard deviation of exit gradient;
$P[i_e > i_{det}]$ = probability that exit gradient will exceed deterministic value;
x, y, z = Cartesian coordinate directions;
α = scaling factor on exit gradient;
θ_k = scale of fluctuation of ln k;
θ_v, θ_h = vertical and horizontal scales of fluctuation;
μ_k, σ_k = target mean and standard deviation of permeability;
μ_{i_e}, σ_{i_e} = mean and standard deviation of exit gradient;
$\mu_{\ln i_e}$, $\sigma_{\ln i_e}$ = mean and standard deviation of logarithm of exit gradient; and
Φ = cumulative normal distribution function.

Performance of Diaphragm Wall Constructed Using Top-Down Method

By Chang-Yu Ou,[1] Member, ASCE, Jui-Tang Liao,[2] and Horn-Da Lin,[3] Member, ASCE

Abstract: This paper presents the performance of an excavation using the top-down construction method. Strut loads, wall displacement, wall bending moment, ground surface settlement, pore-water pressure and bottom heave were measured. Results obtained from those observations are correlated with the construction activities. Field observations indicate that strut loads, wall displacement, and ground surface settlement correspond to those reported in the literature. Bending moments of the wall are studied based on the results of the rebar strain gauge and inclinometer measurements. The supported wall and the soil near the wall have a deep inward movement, which accounts for the magnitude of the lateral earth pressure acting on the wall. The behavior of the supported wall and soil over time is consistent with the variation of pore-water pressure during excavation. Analysis of excavations in soft clay should therefore consider the creep factors and/or pore-water pressure dissipation.

INTRODUCTION

Deep excavation in soft clay normally causes a large wall deflection and large ground surface settlement. Excessive ground surface settlement frequently damages the adjacent property in urban areas. The characteristics of wall deformation and ground movement must be thoroughly understood to protect the adjacent properties. Many investigators have provided studies of case histories, e.g., Karlsrud (1981), Mana and Clough (1981), and Ou et al. (1993), to understand these deformation characteristics. Furthermore, Finno et al. (1989) developed an extensive monitoring program on the Chicago subway excavation HDR-4 project. The observation items included surface and subsurface three-dimensional soil movements, pore-water pressures, sheet-pile deformations, and strut loads. The strength and stress-strain behaviors of the soil at the site were also studied thoroughly (Finno and Nerby 1989). In that case, high pore-water pressures were monitored during the sheet-pile driving, and very large ground movements were observed. This study enhances the knowledge of braced excavations in soft clay.

Most of the cases reported in the literature were constructed using the bottom-up excavation method. This method uses temporary steel struts to support the excavation wall. Installation of the struts requires a relatively short period of time (generally one to two weeks), depending on the size of the excavation. The displacement behavior of the supported wall and soil may change little during the period of strut installation because the pore-water pressure in the clay typically does not dissipate quickly. On the other hand, the top-down excavation method uses concrete floor slabs to support the wall and sometimes requires long periods of time between two successive excavation stages to construct the floor slab. Dissipation of excess pore-water pressure or creep behavior in the soil can have significant effects on the deformation behavior of the wall and soil. For these reasons, a comprehensive monitoring system was installed on the Taipei National Enterprise Center (TNEC) excavation project, which was completed using the top-down construction method. The TNEC structure is an 18-story building and has five basement levels. The site occupies an area of about 3,500 m^2, as shown in Fig. 1. This paper discusses strut loads, wall displacements, wall bending moments, ground movements, pore-water pressures, and bottom heaves associated with construction.

GROUND CONDITIONS

As shown in Fig. 2, the subsurface conditions at the site consist of six layers of alternating silty clay and silty sand deposits overlying a thick gravel formation. The first and second layers are a 5.6-m-thick silty clay (CL) and a 2.4-m-thick silty sand (SM), respectively. The third layer is a 25-m-thick silty clay (CL), and it is mainly this layer that affects the excavation behavior in this case. The liquid limit for this layer of clay ranges from 29 to 39, and the plastic index ranges from 9 to 19. The silt and clay contents are in the range of 40% to 55% and 45% to 60%, respectively. The coefficient of permeability (k) from one-dimensional consolidation tests is around 4×10^{-6} cm/s. The coefficient of consolidation (c_v) ranges between 3×10^{-3} cm^2/s and 1.1×10^{-3} cm^2/s. The fourth and fifth layers are a 2-m-thick medium dense fine sand and 2.5-m-thick medium to stiff clay. The sixth layer is an 8.0-m-thick medium to dense silt or silty sand. A gravel formation is located 46 m below the ground surface and has a standard penetration resistance N value greater than 328 blows/m.

Fig. 3 shows variation of water content, effective overburden pressure, and preconsolidation pressure with depth. The preconsolidation pressure appears to correspond well with the water content. The undrained shear strength was obtained from unconsolidated-undrained (UU) triaxial tests, field vane shear (FV) tests, triaxial K_0-consolidated undrained compression ($CK_0U - AC$) tests, and extension tests ($CK_0U - AE$), as shown in Fig. 4. The drained friction angle (ϕ') equals 30°. In addition, three cone penetration tests with pore-water pressure measurement (CPTU) were performed at the site. The variation in undrained shear strength computed using the formula provided by Roberston and Campanella (1989) from one of the CPTU tests is also shown in Fig. 4, in which the empirical cone factor, N_k, is equal to 15.

Because creep behavior of the silty clay may affect excavation behavior, a series of triaxial compression and lateral extension creep tests was conducted. Both types of these were consolidated isotropically prior to the creep test. Singh and Mitchell's parameters (1968), such as A_1, m, and α, can be obtained from the regression analysis of the test results. The results of the tests indicate that the parameters obtained from lateral extension creep tests are close to those from compression creep tests. This finding implies that the parameters from the compression creep test can be used in the excavation analysis while considering the creep effects, in which lateral de-

[1]Prof., Dept. of Constr. Engrg., National Taiwan Univ. of Sci. and Technol., Taipei, Taiwan, Republic of China.

[2]Grad. Student, Dept. of Constr. Engrg., National Taiwan Univ. of Sci. and Technol., Taipei, Taiwan, Republic of China.

[3]Prof., Dept. of Constr. Engrg., National Taiwan Univ. of Sci. and Technol., Taipei, Taiwan, Republic of China.

Note. Discussion open until February 1, 1999. To extend the closing date one month, a written request must be filed with the ASCE Manager of Journals. The manuscript for this paper was submitted for review and possible publication on February 8, 1996. This paper is part of the ***Journal of Geotechnical and Geoenvironmental Engineering***, Vol. 124, No. 9, September, 1998. ©ASCE, ISSN 1090-0241/98/0009-0798–0808/ $8.00 + $.50 per page. Paper No. 12572.